Title
Copper(I)-Based Highly Emissive All-Inorganic Rare-Earth Halide Clusters

Journal
Matter, 1(1)

ISSN
2590-2393

Authors
Lin, J
Chen, H
Kang, J
et al.

Publication Date
2019-07-10

DOI
10.1016/j.matt.2019.05.027

Peer reviewed

Copper(I) Based Highly Emissive All-Inorganic Rare-Earth Halide Clusters

Jia Lin,[1,3,9] Hong Chen,[1,2,8,9] Jun Kang,[4] Li Na Quan,[1,4] Zhenni Lin,[4,5] Qiao Kong,[1] Minliang Lai,[1] Sunmoon Yu,[4,5] Lei Wang,[7] Lin-wang Wang,[4] Michael F. Toney[2]* and Peidong Yang[1,4,5,6,10]*

[1]Department of Chemistry, University of California, Berkeley, CA 94720, USA

[2]Stanford Synchrotron Radiation Lightsource, SLAC National Accelerator Laboratory, Menlo Park, CA 94025, USA

[3]Department of Physics, Shanghai University of Electric Power, Shanghai 200090, China

[4]Materials Sciences Division, Lawrence Berkeley National Laboratory, Berkeley, CA 94720, USA

[5]Department of Materials Science and Engineering, University of California, Berkeley, CA 94720, USA

[6]Kavli Energy NanoScience Institute, Berkeley, CA 94720, USA

[7]Department of Chemical Engineering, Stanford University, Stanford, CA 94720, USA

[8]School of Environmental Science and Engineering, Southern University of Science and Technology, Shenzhen 518055, China

[9]These authors contributed equally

[10]Lead Contact

*Correspondence: mftoney@slac.stanford.edu (M.F.T.), p_yang@berkeley.edu (P.Y.)

Abstract

The development of new environment-friendly luminescent materials is crucial for future solid-state lighting, sensor, and display applications. Here, a new Cu(I)-based all-inorganic rare-earth halide material, $Rb_8CuSc_3Cl_{18}$, has been synthesized by a solid-state reaction method. In this compound, two Cu(I) ions are connected to three rare-earth halide octahedra to form a paddle-wheel like cluster. Although Sc-based halides are intrinsically non-emissive, the Cu(I) coordinated rare-earth halide clusters in $Rb_8CuSc_3Cl_{18}$ contribute to a strong blue photoluminescence emission with a peak centered at about 473 nm. This Cu(I) regulated emission can also be extended to other isostructural compounds, such as $Rb_8CuY_3Cl_{18}$. Moreover, the crucial role of Cu(I) has been carefully illustrated by replacing Cu(I) with Ag(I) in the isostructural non-emissive $Rb_8AgSc_3Cl_{18}$. Based on comprehensive spectroscopy studies and density function theory calculations, we find that Cu(I) photooxidation and correct orbital energy level alignment are crucial for the observed bright blue emission through a proposed metal (Cu) to octahedra ($[ScCl_6]^{3-}$) charge-transfer mechanism. The discovery of Cu(I)-based all-inorganic rare-earth halide cluster establishes a new strategy for constructing promising emissive halide materials.

Introduction

Halide perovskites are of great interest due to their large potential for a broad range of applications such as photovoltaics (PVs), light-emitting diodes (LEDs), and photodetectors.[1-5] Currently the state-of-the-art highly emissive halide perovskite materials contain toxic lead ions.[6,7] New halide materials with various crystal structures and dimensionalities have been continuously explored in order to discover lead-free alternatives for more efficient and practical optoelectronic applications.[8,9] One of the most explored strategies to design new lead-free halide perovskite compositions is by substituting lead with monovalent B(I) and trivalent B(III) elements based on the $A_2B(I)B(III)X_6$ chemical matrix (where A are the alkali elements, such as Cs^+, Rb^+, K^+, $CH_3NH_3^+$ (MA^+), $HC(NH_2)_2^+$ (FA^+), etc.; B are the different charged metal cations; X are the halide ions) to construct quaternary double B-site halide perovskite analogues, usually denoted as double perovskite "2116" phase. Based on this formula, a series of double perovskites have been discovered based on Ag(I), Au(I) and alkali cations at the B(I) position, such as $Cs_2AgB(III)X_6$ (B(III) = Bi, Sb, In, Tl),[10-13] charge-ordered $Cs_2B(I)B(III)X_6$ (B = Au, Tl),[14,15] and rare-earth based $MA_2KB(III)Cl_6$ (B = Gd, Y).[16,17] These materials offer a broad compositional space as well as interesting physical and optical properties, and thus have potential applications in PVs and X-ray detectors.[10,18] However pristine double perovskite materials are shown to have inferior light emitting characteristics compared to the typical $APbX_3$ halide perovskites,[10] possibly due to the strong localized electric field between the ordered B(I) and B(III) octahedra in the three-dimensional lattice which hinders carrier mobility.

It is well-known that some rare-earth elements, such as Eu^{3+}, Ce^{3+} and Tb^{3+}, can be doped into different halide perovskite matrices to serve as strong light emitting centers for diverse optical applications.[19-22] The emission peak wavelength of the doped matrix does not vary compared to the rare-earth halide salts due to the nature of the intrinsic *d-f* orbital transition. Though the abovementioned rare-earth ions are highly emissive, other rare-earth ions, such as Sc^{3+}, Y^{3+}, and La^{3+}, show weak or no emission in the visible light range, in each case due to an orbital transition

energy mismatch. Since rare-earth ions usually adopt a trivalent state, they can be directly coupled within the double perovskite lattice at the B(III) site.[16] However, these rare-earth based double perovskite structures do not contribute to the improvement of emission properties of these non-emissive rare-earth ions. Thus, a more appropriate sensitizing component is desired in the double B-position configuration in order to construct highly emissive materials from the non-emissive rare-earth halides. Inspired by previous studies, we understand that Cu(I), compared to Ag(I), is not an ideal B(I) cation for constructing halide double perovskites due to the mismatch in coordination and octahedra factor.[23,24] However, it shows excellent sensitizing ability to achieve high light emission in Cu(I) involving metal-organic complexes originating from the metal-to-ligand charge-transfer (MLCT) process.[25-29]

Herein, we successfully obtained a new series of highly emissive all-inorganic double B-site halide materials by combining Cu(I) with the non-emissive rare-earth (Sc, Y) halide octahedra building units in a solid-state reaction synthesis. Although the Sc and Y ions as well as their halide octahedra have no orbital transition emission in the visible light range, after binding these halide octahedra with Cu(I), we obtained compounds $Rb_8CuSc_3Cl_{18}$ and $Rb_8CuY_3Cl_{18}$ which showed greatly enhanced light emission. To understand the emission mechanism, we also replaced Cu(I) with Ag(I) in the isostructural $Rb_8AgSc_3Cl_{18}$, and although $Rb_8CuSc_3Cl_{18}$ and $Rb_8AgSc_3Cl_{18}$ have similar electronic structures, the latter was not emissive. By further combining spectroscopy studies and density function theory (DFT) modeling, we were able to elucidate the underlying mechanism behind Cu(I) enhanced light emission.

Results and Discussion

Synthesis of the series of rare-earth based halide compounds was carried out using the solid-state reaction method in vacuum, which is crucial because it can prevent both Cu(I) oxidization and rare-earth halides hydration in the source materials. RbCl, CuCl or AgCl, and $ReCl_3$ (Re = Sc, Y, La) were weighed based on their stoichiometric ratio in the final products and sealed in a quartz

tube in vacuum. The as-prepared quartz ampoule was then heated in a muffle furnace at 750 °C for 120 hours, and slowly cooled down to room temperature. The detailed preparation procedure is documented in the Supporting Information. After synthesis, the ampoule was cut open in an Ar glove box to obtain small colorless crystals. All characterizations were carried out in air-free conditions, as the obtained materials were hygroscopic and sensitive to air.

Crystal structures of this series of compounds were determined using synchrotron-based single crystal X-ray diffraction (SCXRD) to guarantee high I/sigma data and minimal air exposure for the crystals. As shown in **Figure 1a**, a new halide material, $Rb_8CuSc_3Cl_{18}$, crystallizes in the space group *R*-3*c*, with a = 12.6026(4) Å, c = 74.534(5) Å. Detailed crystallographic parameters and bond distances are summarized in **Table S1, S2**. The asymmetric unit in the crystal structure of $Rb_8CuSc_3Cl_{18}$ consists of two different layers. In one layer isolated $[ScCl_6]^{3-}$ octahedra are separated by Rb^+ cations (**Figure 1b**). In the other layer two Cu(I) ions are linked by three $[ScCl_6]^{3-}$ octahedra that are parallel to one of the $[ScCl_6]^{3-}$ octahedra edges to form a paddle-wheel like $[Cu_2(ScCl_6)_3]^{7-}$ cluster, and the clusters are further separated by Rb^+ cations (**Figure 1c, d**). These two layers are stacked together along the crystallographic *c* axis following the 6_1 symmetry to form a hexagonal structure. The average Sc-Cl bond distance is 2.5 Å in the $[Cu_2(ScCl_6)_3]^{7-}$ cluster, almost equal to that in each isolated $[ScCl_6]^{3-}$ octahedron.

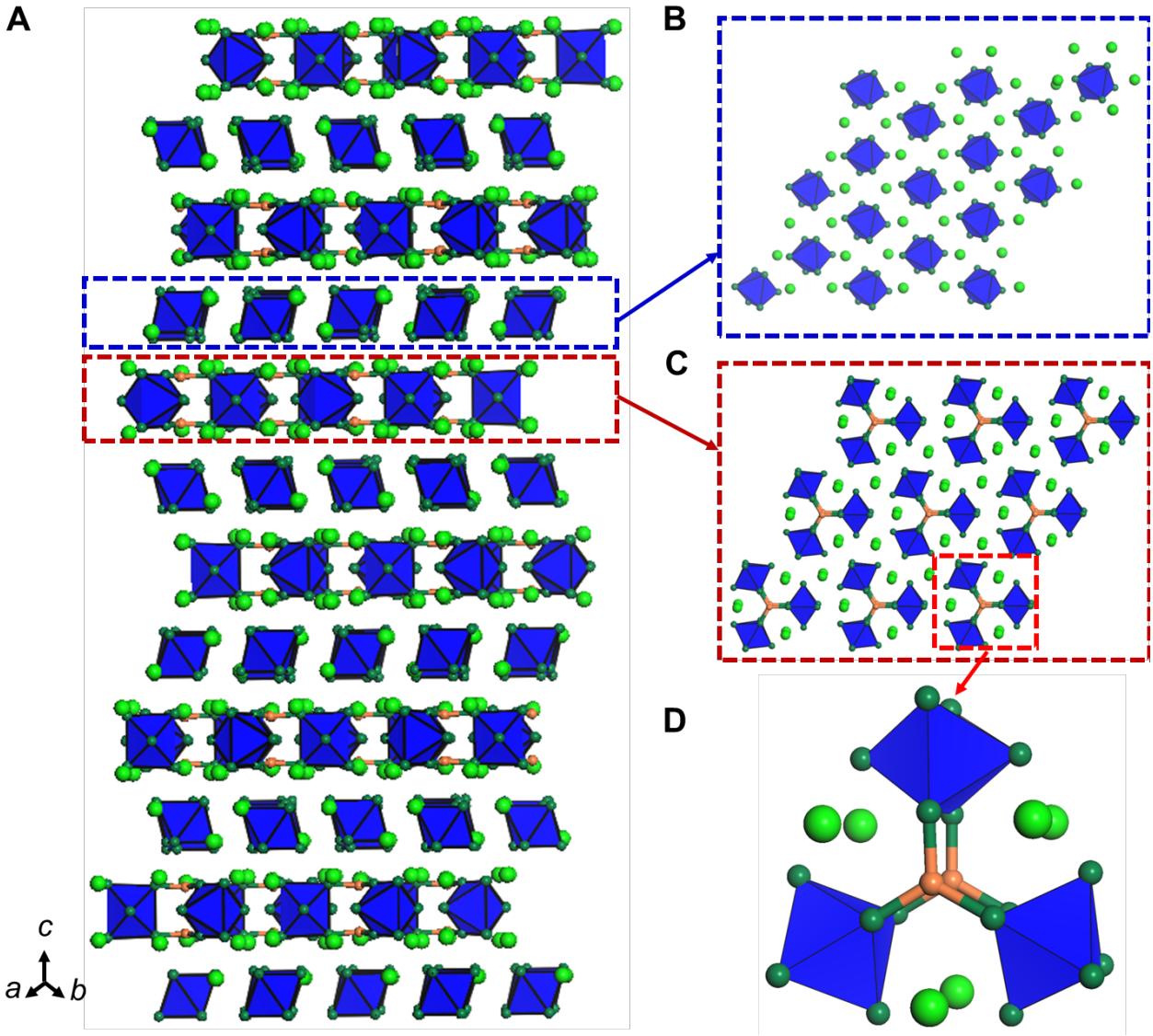

Figure 1. Crystal structure of $Rb_8CuSc_3Cl_{18}$. Crystal structure viewing along (**A**) [110] direction; (**B**) isolated $[ScCl_6]^{3-}$ octahedra layer; (**C**) $[Cu_2(ScCl_6)_3]^{7-}$ cluster layer. (**D**) Zoomed-in view of two 3-coordinated Cu(I) ions connecting three $[ScCl_6]^{3-}$ octahedra to form a $[Cu_2(ScCl_6)_3]^{7-}$ cluster. Light green, dark green, and orange spheres represent Rb, Cl, and Cu atoms, respectively; Sc atoms are in the blue octahedra.

Powder X-ray diffraction (PXRD) was employed to check the purity of the obtained $Rb_8CuSc_3Cl_{18}$ crystals. As this compound is a strong absorber to Cu Kα radiation and is hydroscopic in moisture, high quality PXRD data can only be achieved using synchrotron-based

PXRD in capillary mode, as shown in **Figure 2a**. The experimental PXRD matches well with the simulated pattern, demonstrating the high purity of our sample based on the optimized synthesis recipe. Moreover, X-ray absorption near edge structure (XANES) data was collected to study the oxidation state of Cu ions (**Figure 2b**). $Rb_8CuSc_3Cl_{18}$ shows a very similar edge feature as the CuCl standard, demonstrating the monovalent nature of Cu ions in the obtained crystals. Energy dispersive X-ray spectroscopy (EDX) spectrum shown in **Figure S1** confirms that the atomic ratio of Rb:Cu:Sc:Cl is 8.21:1:2.94:17.14, which is very close to the ideal ratio in the chemical formula obtained from SCXRD refinement. The phase and thermal stability were examined using in-situ temperature-dependent grazing incidence wide angle X-ray scattering (GIWAXS) on dispersed powders under He environment (**Figure 2c, d**). Upon heating from 300 K to 495 K, $Rb_8CuSc_3Cl_{18}$ crystals underwent a thermally induced lattice expansion. The unit cell length in *a* axis expanded by 2.4 % from 12.67 Å to 12.97 Å (expansion coefficient equals to 1.1×10^{-4} K^{-1}), and that in *c* axis expanded by 1.5 % from 75.55 Å to 76.65 Å (expansion coefficient equals to 6.9×10^{-5} K^{-1}), indicating that lattice expansion was anisotropic during heating. The crystalline phase of $Rb_8CuSc_3Cl_{18}$ was stable up to about 500 K, after which the compound started to melt and decompose.

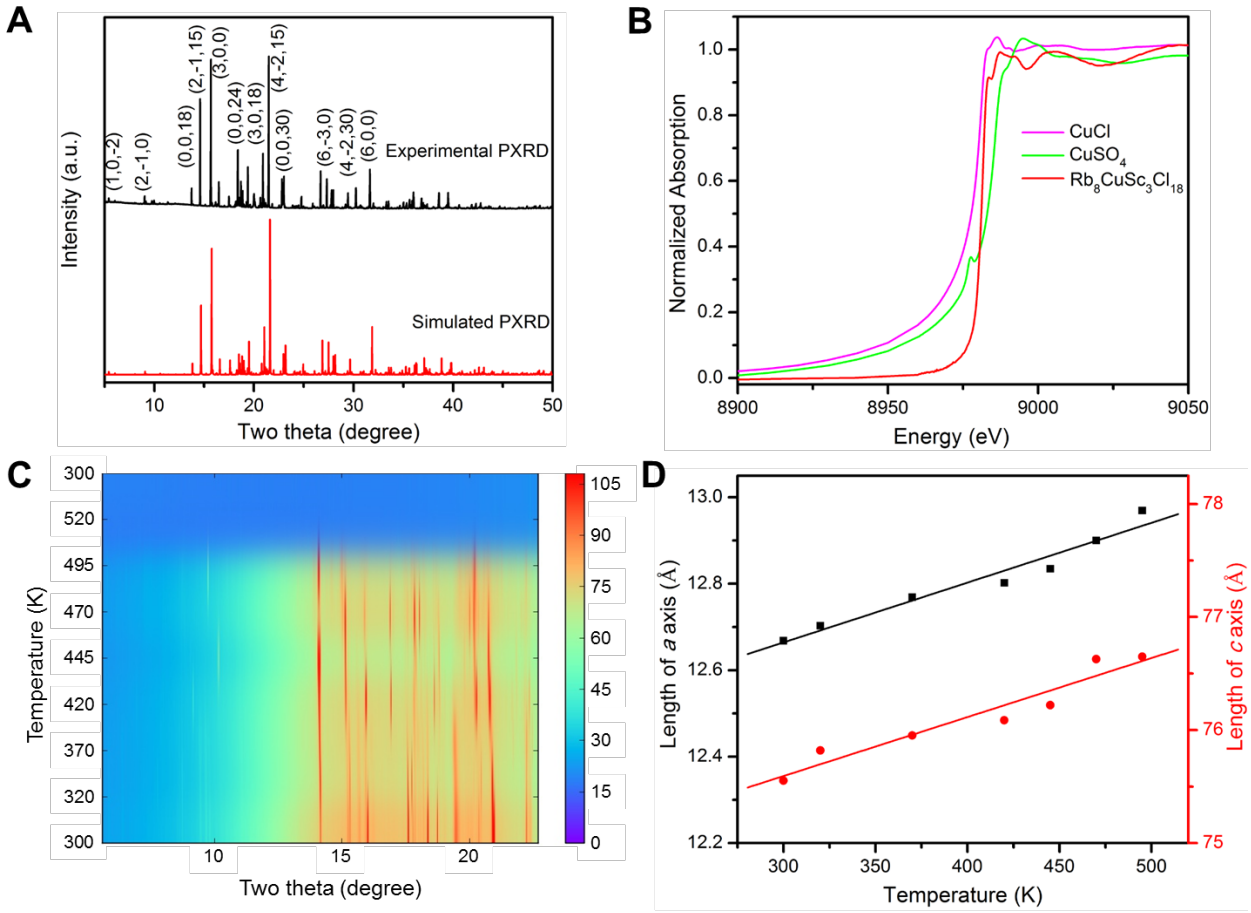

Figure 2. Structural characterizations of $Rb_8CuSc_3Cl_{18}$. (**A**) High-resolution powder X-ray diffraction (PXRD) pattern of the as-synthesized $Rb_8CuSc_3Cl_{18}$ powder with synchrotron radiation under capillary mode (λ = 0.999 Å). (**B**) Cu K-edge X-ray absorption near edge structure (XANES) data. (**C**) In-situ temperature-dependent grazing incidence wide angle X-ray scattering (GIWAXS) in He atmosphere and (**D**) unit cell parameters and the linear fitting.

Although there have been extensive studies on Cu(I) involving hybrid inorganic-organic and all-inorganic materials for their emissive properties,[25-31] 3-coordinated Cu(I)-incorporated all-inorganic compounds with high emission have not been reported. Here, a highly blue-emissive feature under UV light excitation has been observed for $Rb_8CuSc_3Cl_{18}$. Detailed characterization of the photoluminescence (PL) property of this material is illustrated in **Figure 3a**. Under excitation of a 375 nm laser, the crystal shows a strong and relatively broad PL emission, with its peak wavelength centering at around 473 nm. The peak can be fitted using a Gaussian function

with a full-width-of-half-maximum (FWHM) of 69.1 nm (**Figure S2**). The PL quantum yield (PLQY) of the solid-state single crystal was measured about 7.95 %, a high value as compared with bulk lead halide perovskites, for example, $CsPbX_3$ with PLQY less than 1 %.[32] We further converted the PL emission pattern to the calculated chromaticity on a CIE1931 color diagram, as shown in **Figure 3b**. The chromaticity of the emission is located at (0.15, 0.20), which is close to that of the pure blue color at (0.15, 0.06) used in standard Red Green Blue (sRGB) gamut, indicating the potential application of $Rb_8CuSc_3Cl_{18}$ as a highly efficient blue-emissive material. The measured UV-Vis spectrum (**Figure 3c**) shows a sharp edge and an absorption maximum at about 366 nm. By further converting the absorption spectrum into a Tauc plot, we obtained an optical bandgap of 3.10 eV for $Rb_8CuSc_3Cl_{18}$, which deviates significantly from the PL emission peak energy (2.62 eV). This observation indicates that PL of this compound is not originated from the band edge emission, unlike most of the halide perovskite materials. Time-resolved PL decay curve of $Rb_8CuSc_3Cl_{18}$ (**Figure 3d**) shows a bi-exponential decay trace. By fitting the curve, we determined the carrier recombination lifetimes to be $\tau_1 = 1.63$ ns and $\tau_2 = 4.92$ ns, similar to values found in the typical halide perovskite materials[33] but are much shorter than those found in rare-earth doped phosphors which have lifetimes greater than microseconds. From the PL spectra at room temperature and 4 K shown in **Figure S3**, we did not observe any significant change in the spectral profile, peak wavelength, and peak intensity, indicating that the radiative process is not strongly affected by temperature.

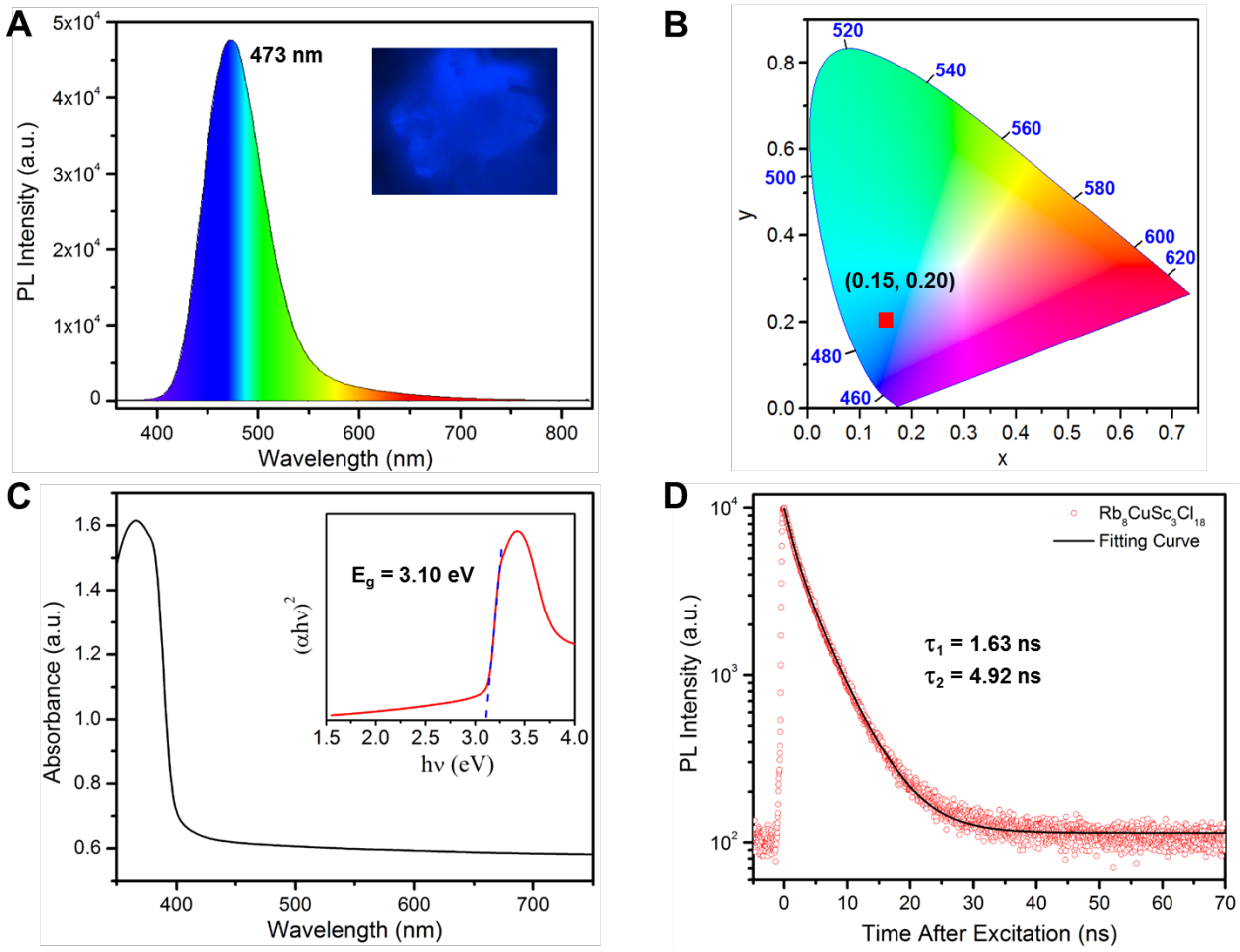

Figure 3. Optical properties of $Rb_8CuSc_3Cl_{18}$. (**A**) Solid-state photoluminescence (PL) spectrum and PL image (inset). (**B**) Chromaticity of the emission extracted from the PL spectrum. (**C**) UV-Vis absorption spectrum and the corresponding Tauc plot (inset). (**D**) Time-resolved PL decay measurement at 473 nm, the emission wavelength.

The effectiveness of constructing Cu 3-coordinated halide compounds is further exemplified by the preparation of the isostructural $Rb_8CuY_3Cl_{18}$ under similar synthesis conditions. The unit cell lengths, a = 12.8945(12) Å and c = 75.684(11) Å, are 2.32 % and 1.54 % longer than those of $Rb_8CuSc_3Cl_{18}$, respectively. The detailed structure parameters are presented in **Table S1**. The Cu···Cu distance in $Rb_8CuY_3Cl_{18}$ is 3.561 Å, which is significantly longer than that in $Rb_8CuSc_3Cl_{18}$ (3.116 Å) due to the larger ionic radius of Y^{3+}. Both compounds have the same Cu-Cl bond distance of 2.254 Å (**Figure S4**). EDX spectrum of a $Rb_8CuY_3Cl_{18}$ single crystal

determines its atomic ratio to be 8.23:1:2.81:17.44, which is very close to the ideal stoichiometric ratio (**Figure S5**). The PL emission of $Rb_8CuY_3Cl_{18}$ is centered around 493 nm (PLQY = 5.26 %, **Figure S6**), slightly red shifted compared to $Rb_8CuSc_3Cl_{18}$. DFT calculations show that $Rb_8CuY_3Cl_{18}$ has a larger band gap than $Rb_8CuSc_3Cl_{18}$ (**Figure S7**). This is consistent with the larger optical band gap of 3.61 eV of $Rb_8CuY_3Cl_{18}$ derived from the absorption spectrum (**Figure S8**), further indicating that the PL of this series of compounds is not from the band-edge emission. We notice that although optically the as-synthesized $Rb_8CuY_3Cl_{18}$ exhibits a single emission peak, PXRD of $Rb_8CuY_3Cl_{18}$ shows several extra diffraction peaks (**Figure S9**). It is hypothesized that due to its strong hydration, this material can react with a trace amount of water quickly during processing and measurement, forming products that contribute to the appearance of the unknown PXRD diffraction peaks. In-situ ambient pressure XPS (AP-XPS) study further indicates that after exposure to oxygen, the oxidized copper divalent state can be formed at the surface of the compound, indicating the sensitivity of this material to oxidation, as shown in **Figure S10**. Going further down the periodic table in an attempt to replace B(III) position with even larger radius La^{3+} ions, we can only obtain Rb_2LaCl_5 with a one-dimensional chain-like crystal structure (see **Figure S11**), which crystallizes in the space group *Pnma*, with a = 13.0254(5) Å, b = 8.9939(3) Å, c = 8.1427(3) Å (**Table S1**). PXRD pattern of the sample with expected composition of $Rb_8CuLa_3Cl_{18}$ mainly showed Rb_2LaCl_5 diffraction peaks and a small amount of Rb_2CuCl_3 impurity (**Figure S12**). A possible explanation is that the ionic radius of La^{3+}, as compared to those of Sc^{3+} and Y^{3+} ions, is too large to be compatible in the present structure motif.[34,35]

To further analyze the light emission properties of $Rb_8CuSc_3Cl_{18}$, we carried out PL experiments in an inert atmosphere for all the source materials used in synthesis. As shown in **Figure 4a** and **Figure S13**, under the same excitation conditions, the source materials, CuCl and RbCl, both showed negligible emission. $ScCl_3$ showed very weak emission (~ 1/129 intensity, measured with same laser power and sample area) and a different peak wavelength (around 455 nm) compared to $Rb_8CuSc_3Cl_{18}$. These results excluded the possibility of emission from either the

source materials or the orbital transitions reported frequently in rare-earth ions doped materials. Besides orbital transitions, crystal-field regulated PL has also been reported in materials involving rare-earth ions.[36,37] To understand the emission mechanism, we synthesized another Sc-involved halide compound, $Rb_3Sc_2Cl_9$, and characterized its PL under the same excitation condition. As shown in **Figure S14**, although the Sc atoms are coordinated with six chloride ions in the octahedral environment with similar average bond distance of 2.5 Å as in $Rb_8CuSc_3Cl_{18}$, $Rb_3Sc_2Cl_9$ shows much weaker and broader emission.[38,39] In this sense, it is difficult to ascribe crystal-field effect alone to be responsible for the high emission of our new material; the highly emissive feature must involve the contribution from Cu(I).

To gain more insight into the mechanism behind the experimental observations, we carried out DFT calculations to probe the electronic structure and density of states (DOS) of $Rb_8CuSc_3Cl_{18}$. As shown in **Figure S15**, the Cu *d* orbital dominates near the top of the valence band and the valence band maximum (VBM), while the Sc *d* orbital mainly contributes to the conduction band and the conduction band minimum (CBM). The band structure of this compound shows negligible band dispersion. The $[ScCl_6]^{3-}$ octahedra are almost isolated from each other in the compound and thus their coupling is negligible, leading to a nearly flat conduction band, a feature commonly found in quasi-zero dimensional perovskites.[40-42] It is widely reported that the luminescence properties of 2-, 3-, or 4-coordinated Cu(I) hybrid metal-organic complexes strongly depend on the intersystem crossing (ISC) processes.[27,43] Here, the $[ScCl_6]^{3-}$ octahedra in $Rb_8CuSc_3Cl_{18}$ play a similar role as the ligands in metal-organic complexes. The proposed emission process is depicted in **Figure 4b**. Upon excitation the Cu(I) ions can be oxidized to become Cu(II)* with electron transfer from Cu to $[ScCl_6]^{3-}$ octahedra in the cluster in the emissive state,[44] leading to the bright blue and relatively broad emission in the PL spectrum. This emission position depends on the type of halide octahedra connected with Cu(I). We refer to this as a metal (Cu) to halide octahedra ($[ScCl_6]^{3-}$) charge transfer process. The phenomenon of emission from part of the

structure is similar with that observed in the organic-inorganic Pb-Cl assembly reported recently, where only trimer clusters in the structure contribute to emission.[45]

Since Cu(I) as a monovalent element is so crucial to enhance PL emission in this complicated structure, other monovalent elements might possibly have similar effects. To explore this hypothesis, we also tried to replace Cu(I) with Ag(I), which is a d^{10} monovalent metal ion as well. As confirmed by SCXRD, the $Rb_8AgSc_3Cl_{18}$ single crystals can be successfully obtained using the similar synthesis strategy. It crystallizes as the isostructure of the Cu analogue with the space group *R*-3*c* and unit cell dimensions of a = 12.5904(4) Å and c = 74.856(3) Å (**Table S1**). The unit cell is similar to that obtained for the Cu version. Detailed structural analysis shows that Ag(I) cations are refined to locate in three disordered positions. In one of the disordered species the Ag-Cl bond distance is 2.264 Å, which is very similar to the Cu-Cl bond distance of 2.254 Å (**Figure 4c, d**). Moreover, Ag(I) ions also adopt a 3-coordination environment like Cu(I). Compared with the Cu···Cu distances of 3.116 Å and 3.561 Å in $Rb_8CuSc_3Cl_{18}$ and $Rb_8CuY_3Cl_{18}$, respectively, the Ag···Ag distance of 4.212 Å in $Rb_8AgSc_3Cl_{18}$ is considerably larger. This leads to a weaker inter-metallic interaction between the two Ag atoms compared to that between the Cu atoms pairs. Further PL experiments showed that emission from this Ag(I) coordinated Sc-Cl octahedra was not detectable. Also, the $Rb_8AgSc_3Cl_{18}$ powder gradually changed color from white to gray under UV light excitation, indicating that this compound was susceptible to photodecomposition. DFT calculations of $Rb_8AgSc_3Cl_{18}$ show a similar band structure as the Cu counterpart (**Figure S16**). Ag(I) has a higher oxidation potential and thus can be easily reduced to Ag(0) under excitation, which possibly hinders charge transfer between Ag and the octahedra, resulting in poor emission.[46,47] This study indicates that although from a crystallographic point of view isoelectronic Ag(I) can replace the Cu(I) position resulting in similar Cu-Cl and Ag-Cl bond distances and coordination environment, the optical properties are heavily dependent on the orbital locations of the excited states of these cations.

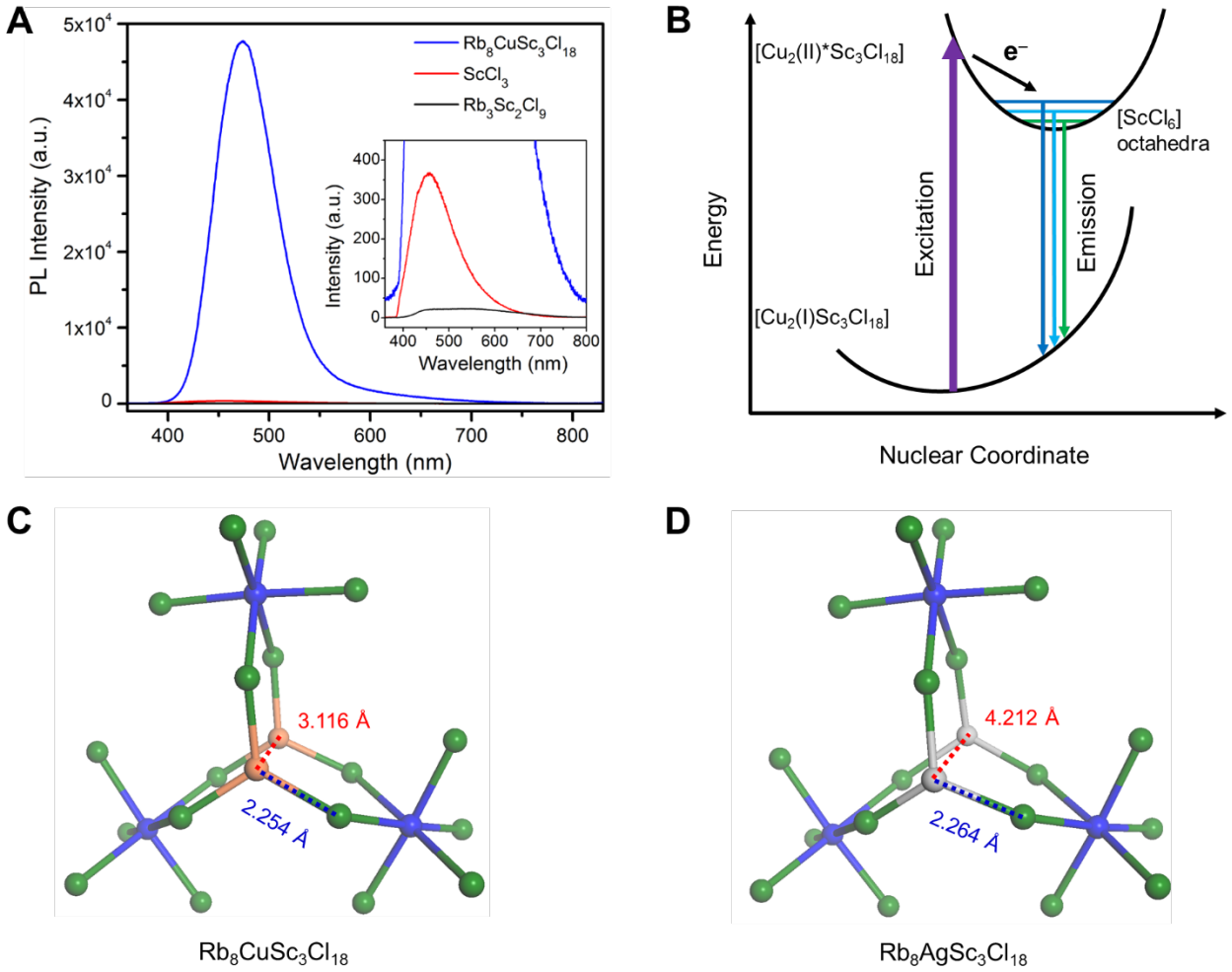

Figure 4. Emission mechanism of $Rb_8CuSc_3Cl_{18}$. (**A**) PL spectra of $Rb_8CuSc_3Cl_{18}$ (blue), $ScCl_3$ (red) and $Rb_3Sc_2Cl_9$ (black). (**B**) Schematic energy level diagram showing the PL emission mechanism. (**C, D**) Comparison of the Cu-Cl and Ag-Cl bond distances and Cu···Cu and Ag···Ag interaction distances in the $[Cu_2Sc_3Cl_{18}]^{7-}$ and $[Ag_2Sc_3Cl_{18}]^{7-}$ clusters in Cu(I)- and Ag(I)- involved isostructures. Dark green, blue, orange and gray spheres represent Cl, Sc, Cu and Ag atoms, respectively.

3. Conclusions

In this work, we discovered a highly emissive all-inorganic Cu(I)-containing rare-earth halide compound $Rb_8CuSc_3Cl_{18}$. In this structure, the Cu(I) ions show a 3-coordination geometry with the halide ions and they connect Sc-Cl octahedra to form clusters in alternating layers. High PL intensity blue emission has been observed in this compound in solid state at room temperature. We have also found similar highly emissive features in other isostructural compounds, such as $Rb_8CuY_3Cl_{18}$. To demonstrate the crucial role of Cu(I) on the regulation of the electronic structure and emission properties of this series of rare-earth halide cluster compounds, the Cu(I) was replaced with Ag(I), and the obtained isostructural compound $Rb_8AgSc_3Cl_{18}$ was found to be non-emissive. Based on this structure matrix, we demonstrate that Cu(I) can enhance the optical emission of the non-emissive rare-earth ions in the newly discovered Cu-halide octahedra clusters with metal to halide octahedra charge transfer characteristics. We expect that the Cu(I)-enhanced emission in these new all-inorganic rare-earth-based halide materials can be extended to other rare-earth ions to realize wide range of optical properties, promising for lead-free light-emitting applications.

Supplemental Information

Supplemental Information can be found online.

Synthesis and characterization, X-ray crystallography, and DFT calculations, including Figures S1-S17, and Tables S1, S2.

X-ray crystallography data for $Rb_8CuSc_3Cl_{18}$, $Rb_8CuY_3Cl_{18}$, $Rb_8AgSc_3Cl_{18}$, and Rb_2LaCl_5.

Author Contributions

J.L., H.C., M.F.T. and P.Y. conceived the idea and designed the study. J.L. and H.C. contributed to the experimental work. L.N.Q., Z.L. and M.L. helped with the optical characterizations. J.K. and L.W. performed the DFT modeling. Q.K. performed the EDX measurement. S.Y. and L.W. performed the XPS characterizations. J.L., H.C., M.F.T. and P.Y. wrote the manuscript. All authors discussed the results and revised the manuscript.

Declaration of Interests

The authors declare no competing interests.

Highlights

A new series of all-inorganic halide cluster structured materials were discovered

The first 3-coordinated Cu(I)-containing all-inorganic halide compound were demonstrated

Cu(I) enhanced blue emission in the rare-earth-based halide materials was observed

Acknowledgements

This work was supported by the U.S. Department of Energy, Office of Science, Office of Basic Energy Sciences, Materials Sciences and Engineering Division, under contract DE-AC02-05CH11231 within the Physical Chemistry of Inorganic Nanostructures Program (KC3103). Simon Teat and Laura McCormick are acknowledged for help on accommodating the single crystal X-ray beamtime. The research used resource at the Stanford Synchrotron Radiation Lightsource at SLAC National Accelerator Laboratory supported by the U.S. Department of Energy, Office of Science, Basic Energy Sciences under contract no. DE-AC02-76SF00515, including PXRD at beamline 2-1, GIWAXS at beamline 11-3, and XANES at beamline 2-2. This research also used resource of the Advanced Light Source, which is a DOE Office of Science User Facility under contract no. DE-AC02-05CH11231, including SCXRD at beamline 12.2.1, and AP-XPS at beamline 9.3.2. The computational resources are provided by the National Energy Research Scientific Computing Center and the Oak Ridge Leadership Computing Facility through the INCITE project. H.C. acknowledges the postdoctoral scholarship support from the Wallenberg Foundation through the MAX IV synchrotron radiation facility program. J.L. acknowledges the fellowship support from Shanghai University of Electric Power. M.F.T. gratefully acknowledges support from the Center for Hybrid Organic Inorganic Semiconductors for Energy (CHOISE) an Energy Frontier Research Center funded by the Office of Basic Energy Sciences, Office of Science within the U.S. Department of Energy through contract number DE-AC36-08G028308.

References:

1 Green, M. A. & Ho-Baillie, A. Perovskite solar cells: the birth of a new era in photovoltaics. *ACS Energy Lett.* **2**, 822–830 (2017).

2 Correa-Baena, J.-P. *et al.* The rapid evolution of highly efficient perovskite solar cells. *Energy Environ. Sci.* **10**, 710–727 (2017).

3 Becker, M. A. *et al.* Bright triplet excitons in caesium lead halide perovskites. *Nature* **553**, 189–193 (2018).

4 Gong, X. *et al.* Electron–phonon interaction in efficient perovskite blue emitters. *Nat. Mater.* **17**, 550–556 (2018).

5 Ahmadi, M., Wu, T. & Hu, B. A review on organic–inorganic halide perovskite photodetectors: device engineering and fundamental physics. *Adv. Mater.* **29**, 1605242 (2017).

6 Lin, K. *et al.* Perovskite light-emitting diodes with external quantum efficiency exceeding 20 per cent. *Nature* **562**, 245–248 (2018).

7 Cao, Y. *et al.* Perovskite light-emitting diodes based on spontaneously formed submicrometre-scale structures. *Nature* **562**, 249–253 (2018).

8 Abate, A. Perovskite solar cells go lead free. *Joule* **1**, 659–664 (2017).

9 Lyu, M., Yun, J. H., Chen, P., Hao, M. & Wang, L. Addressing toxicity of lead: progress and applications of low-toxic metal halide perovskites and their derivatives. *Adv. Energy Mater.* **7**, 1602512 (2017).

10 Slavney, A. H., Hu, T., Lindenberg, A. M. & Karunadasa, H. I. A bismuth-halide double perovskite with long carrier recombination lifetime for photovoltaic applications. *J. Am. Chem. Soc.* **138**, 2138–2141 (2016).

11 Tran, T. T., Panella, J. R., Chamorro, J. R., Morey, J. R. & McQueen, T. M. Designing indirect–direct bandgap transitions in double perovskites. *Mater. Horiz.* **4**, 688–693 (2017).

12 Volonakis, G. *et al.* $Cs_2InAgCl_6$: A new lead-free halide double perovskite with direct band gap. *J. Phys. Chem. Lett.* **8**, 772–778 (2017).

13 Slavney, A. H. *et al.* Small-bandgap halide double perovskites. *Angew. Chem. Int. Ed.*, **57**, 12765–12770 (2018).

14 Eijndhoven, J. T.-v. & Verschoor, G. Redetermination of the crystal structure of $Cs_2AuAuCl_6$. *Mater. Res. Bull.* **9**, 1667–1670 (1974).

15 Retuerto, M. *et al.* Synthesis and properties of charge-ordered thallium halide perovskites, $CsTl^{+}_{0.5}Tl^{3+}_{0.5}X_3$ (X= F or Cl): theoretical precursors for superconductivity? *Chem. Mater.* **25**, 4071–4079 (2013).

16 Deng, Z. *et al.* Synthesis and characterization of the rare-earth hybrid double perovskites: $(CH_3NH_3)_2KGdCl_6$ and $(CH_3NH_3)_2KYCl_6$. *J. Phys. Chem. Lett.* **8**, 5015–5020 (2017).

17 Meyer, G. The synthesis and structures of complex rare-earth halides. *Prog. Solid State Chem.* **14**, 141–219 (1982).

18 Pan, W. *et al.* $Cs_2AgBiBr_6$ single-crystal X-ray detectors with a low detection limit. *Nat. Photonics* **11**, 726–732 (2017).

19 Pan, G. *et al.* Doping lanthanide into perovskite nanocrystals: highly improved and expanded optical properties. *Nano Lett.* **17**, 8005–8011 (2017).

20 Cheng, Y., Shen, C., Shen, L., Xiang, W. & Liang, X. Tb^{3+}, Eu^{3+} co-doped $CsPbBr_3$ QDs glass with highly stable and luminous adjustable for white LEDs. *ACS Appl. Mater. Interfaces* **10**, 21434–21444 (2018).

21 Hu, Q. *et al.* Rare earth ion-doped $CsPbBr_3$ nanocrystals. *Adv. Opt. Mater.* **6**, 1700864 (2018).

22 Yao, J.-S. *et al.* Ce^{3+}-doping to modulate photoluminescence kinetics for efficient $CsPbBr_3$ nanocrystals based light-emitting diodes. *J. Am. Chem. Soc.* **140**, 3626–3634 (2018).

23 Xiao, Z., Du, K. Z., Meng, W., Mitzi, D. B. & Yan, Y. Chemical origin of the stability difference between ccopper (I)-and silver (I)-based halide double perovskites. *Angew. Chem. Int. Ed.* **56**, 12107–12111 (2017).

24 Filip, M. R., Liu, X., Miglio, A., Hautier, G. & Giustino, F. Phase diagrams and stability of lead-free halide double perovskites $Cs_2BB'X_6$: B = Sb and Bi, B' = Cu, Ag, and Au, and

X = Cl, Br, and I. *J. Phys. Chem. C* **122**, 158–170 (2017).

25 Evariste, S. *et al.* Adaptive coordination-driven supramolecular syntheses toward new polymetallic Cu(I) luminescent assemblies. *J. Am. Chem. Soc.* **140**, 12521–12526 (2018).

26 Cariati, E. *et al.* Cu(I) hybrid inorganic–organic materials with intriguing stimuli responsive and optoelectronic properties. *Coord. Chem. Rev.* **306**, 566–614 (2016).

27 Hamze, R. *et al.* Eliminating nonradiative decay in Cu(I) emitters: >99% quantum efficiency and microsecond lifetime. *Science* **363**, 601–606 (2019).

28 Hofbeck, T., Monkowius, U. & Yersin, H. Highly efficient luminescence of Cu(I) compounds: thermally activated delayed fluorescence combined with short-lived phosphorescence. *J. Am. Chem. Soc.* **137**, 399–404 (2015).

29 Cuttell, D. G., Kuang, S.-M., Fanwick, P. E., McMillin, D. R. & Walton, R. A. Simple Cu(I) complexes with unprecedented excited-state lifetimes. *J. Am. Chem. Soc.* **124**, 6–7 (2002).

30 Jun, T. *et al.* Lead-Free Highly Efficient Blue-Emitting $Cs_3Cu_2I_5$ with 0D Electronic Structure. *Adv. Mater.* **30**, 1804547 (2018).

31 Roccanova, R. *et al.* Near-Unity Photoluminescence Quantum Yield in Blue-Emitting $Cs_3Cu_2Br_{5-x}I_x$ ($0 \leqslant x \leqslant 5$). *ACS Appl. Electron. Mater.* **1**, 269–274 (2019).

32 Quan, L. N. *et al.* Highly emissive green perovskite nanocrystals in a solid state crystalline matrix. *Adv. Mater.* **29**, 1605945 (2017).

33 Yang, B. *et al.* Lead-free direct band gap double-perovskite nanocrystals with bright dual-color emission. *J. Am. Chem. Soc.* **140**, 17001–17006 (2018).

34 Jia, Y. Crystal radii and effective ionic radii of the rare earth ions. *J. Solid State Chem.* **95**, 184–187 (1991).

35 Barrett, S. D. & Dhesi, S. S. *The structure of rare-earth metal surfaces*. (World Scientific, 2001).

36 Ronda, C., Jüstel, T. & Nikol, H. Rare earth phosphors: fundamentals and applications. *J. Alloys Compd.* **275**, 669–676 (1998).

37 Ofelt, G. Intensities of crystal spectra of rare-earth ions. *J. Chem. Phys.* **37**, 511–520 (1962).

38 Klemm, W. & Krose, E. Die Kristallstrukturen von $ScCl_3$, $TiCl_3$ und VCl_3. *Zeitschrift für anorganische Chemie* **253**, 218–225 (1947).

39 Meyer, G. & Schönemund, A. Enneahalodimetallates (III) of rare earth elements with the hexagonal $Cs_3Tl_2Cl_9$-$(h)_6$-type structure. *Mater. Res. Bull.* **15**, 89–94 (1980).

40 Xiao, Z., Meng, W., Wang, J., Mitzi, D. B. & Yan, Y. Searching for promising new perovskite-based photovoltaic absorbers: the importance of electronic dimensionality. *Mater. Horiz.* **4**, 206–216 (2017).

41 Yin, J. *et al.* Molecular behavior of zero-dimensional perovskites. *Sci. Adv.* **3**, e1701793 (2017).

42 Yin, J. *et al.* Point defects and green emission in zero-dimensional perovskites. *J. Phys. Chem. Lett.* **9**, 5490–5495 (2018).

43 Khatri, N. M. *et al.* Luminescence and nonlinear optical properties in copper(I) halide extended networks. *Inorg. Chem.* **55**, 11408–11417 (2016).

44 Armaroli, N. Photoactive mono-and polynuclear Cu(I)–phenanthrolines. A viable alternative to Ru(II)–polypyridines? *Chem. Soc. Rev.* **30**, 113–124 (2001).

45 Zhou, C. *et al.* Blue emitting single crystalline assembly of metal halide clusters. *J. Am. Chem. Soc.* **140**, 13181–13184 (2018).

46 Oshio, H. & Ito, T. Assembly of imino nitroxides with Ag(I) and Cu(I) ions. *Coord. Chem. Rev.* **198**, 329–346 (2000).

47 Hsu, C.-W. *et al.* Systematic investigation of the metal-structure–photophysics relationship of emissive d^{10}-complexes of group 11 elements: the prospect of application in organic light emitting devices. *J. Am. Chem. Soc.* **133**, 12085–12099 (2011).